Nuclear Engineering and Technology 52 (2020) 1611–1625

Contents lists available at ScienceDirect

Nuclear Engineering and Technology

journal homepage: www.elsevier.com/locate/net

Original Article

Design of A scale-down experimental model for SFR reactor vault cooling system performance analyses

Koung Moon Kim [a], Ji-Hwan Hwang [b], Somchai Wongwises [c], Dong-Wook Jerng [b, **], Ho Seon Ahn [a, *]

[a] Department of Mechanical Engineering, Incheon National University, Incheon, Republic of Korea
[b] School of Energy System Engineering, Chung-Ang University, Seoul, Republic of Korea
[c] Department of Mechanical Engineering, King Mongkut's University of Technology Thonburi, Thailand

ARTICLE INFO

Article history:
Received 1 October 2019
Received in revised form
2 December 2019
Accepted 8 January 2020
Available online 13 January 2020

Keywords:
Scaling analysis
Natural convection
Vertical parallel plate
Asymmetric heating
RVCS

ABSTRACT

We propose a scaled-down experimental model of vertical air-natural convection channels by applying the modified Ishii–Kataoka scaling method with the assistance of numerical analyses to the Reactor Vault Cooling System (RVCS) of the Proto-type Gen-IV Sodium-cooled fast reactor (PGSFR) being developed in Korea. Two major non-dimensional numbers (modified Richardson and Friction number) from the momentum equation and Stanton number from the energy balance equation were identified to design the scaled-down experimental model to assimilate thermal-hydraulic behaviors of the natural convective air-cooling channel of RVCS. The ratios of the design parameters in the PGSFR RVCS between the prototype and the scaled-down model were determined by setting Richardson and Stanton number to be unity. The friction number which cannot be determined by the Ishii-Kataoka method was estimated by numerical analyses using the MARS-KS system code. The numerical analyses showed that the friction number with the form loss coefficient of 2.0 in the scale-down model would result in an acceptable prediction of the thermal-hydraulic behavior in RVCS. We also performed experimental benchmarking using the scaled-down model with the MARS-KS simulations to verify the appropriateness of the scale-down model, which demonstrated that the temperature rises and the average air flow velocity measured in the scale-down model.

1. Introduction

The Prototype Gen-IV Sodium-cooled Fast Reactor (PGSFR) is one of the Generation IV Reactors (Gen-IV) that is currently under development by the Korea Atomic Energy Research Institute (KAERI) [1]. A primary method of keeping nuclear reactors safe is to remove the decay heat via reliable methods. Therefore, the PGSFR is equipped with two decay heat removal systems to remove the decay heat under design based accident (DBA) conditions. In addition, there is a reactor vault cooling system (RVCS) that is designed to maintain the integrity of the concrete structure surrounding the reactor vessel during thermal damage [2,3]. In addition, the RVCS is a passive air-cooling system that can enhance the inherent safety by removing decay heat through natural convection of airflow in case the two decay heat removal systems are unavailable under unexpected accidents. Therefore, predicting the heat removal performance of RVCSs by natural convection under the inoperable conditions of the decay heat removal systems is important. Fig. 1 shows a schematic image of the RVCS.

RVCS is a U-shaped air channel that encloses both the outer surface of the containment vessel (CV) and the inner surface of the concrete wall containing the separator (SP) between them. Cold air flows through the downcomer channel into the annular region between the SP wall and the reactor housing concrete structure. The air is heated while it passes through the riser channel, which is surrounded by the CV and SP wall before flowing out to the atmosphere [2].

This natural convection flow and heat transfer depend on geometrical factors, such as downcomer and riser-channel configurations, and thermal conditions such as the temperature of the inlet cold air, the heat from the reactor vessel, and the heat radiated from the outer wall of CV to the inner wall of SP. CV could be a heat

* Corresponding author.
** Corresponding author.
E-mail addresses: dwjerng@cau.ac.kr (D.-W. Jerng), hsahn@inu.ac.kr (H.S. Ahn).

https://doi.org/10.1016/j.net.2020.01.005

Nomenclature

a	Area m^2
d	Diameter, Gap size m
f	Friction factor
g	Gravitational acceleration m/s^2
h	Convective heat transfer coefficient W/m^2 K
k	Thermal conductivity W/m K
l	Length (height) m
q''	Heat flux W/m^2
t	Time sec
u_{avg}	Average velocity m/s
v	Volume m^3
A	Area ratio ($A_i = a_i/a_0$)
C_p	Specific heat J/kg K
F	Friction term(fl/d)
K	Form (minor) loss coefficient
Q	Heat rate ($Q = aq''$) W
T	Temperature °C
U	Average velocity ratio, uncertainty

Greek symbols

β	Thermal expansion ratio
ρ	Density kg/m^3
τ	Time ratio
θ	Temperature ratio $(T\text{-}T_{in})/(T_{out}\text{-}T_{in})$

Subscripts

Conv	Convection
Cross	Cross section
f	Fluid
h	Heated section
i	*i* th section
o	Reference
R	Ratio between model and prototype
Rad	Radiation
r	Reference (Heated section)
s	Solid (heated section)
t	Thermal (power)
w	Wall
Out	Outlet
In	Inlet

source causing the airflow in the riser channel by natural convection. From CV, the convective heat is directly transferred to the air in the riser channel. However, the radiative heat across the airflow from CV to SP should be considered because of the high temperature (750 K) of CV. Because the side of SP opposite to the airflow is thermally insulated, it would be reasonable that the heat transferred by radiation from CV could be transferred to the airflow in the riser channel again. Thus, the complex heat transfer modes from CV by convection and radiation can be simplified into the convective heat transfer problem from the heated walls on both sides of CV and inner SP as shown in Fig. 2.

Briefly, the main purpose of this study is to analyze the natural convection heat transfer problem with one heat source (CV) and one heat sink (airflow); however, the heat from the heat source is transferred because of radiation and natural convection, which is a complicated heat transfer process.

Numerous previous studies on the RVCS have investigated the heat transfer performance by natural convection. Choi et al. [4] analyzed the sensitivity of design parameters (such as chimney height, gap size between CV and SP, chimney hydraulic diameter, and emissivity) of RVCS using the multi-dimensional analysis of reactor safety-liquid metal reactor (MARS-LMR) code. They reported that the gap size of the riser section is the most sensitive design parameter affecting the heat removal rate of RVCS. Heineman et al. [5] studied the RVCS of the Power Reactor Innovative Small Module (PRISM), which is a small sodium-cooled fast reactor with a large-scale test apparatus. They performed experiments under conditions of either uniform heat flux (1.8–15 kW/m^2) or uniform wall temperature (200–400 °C) in a heated section with a height of approximately 6.7 m. Dittus-Boelter correlations used for forced convection were applied. Cheng et al. [6,7] studied a passive cooling system for the AP600 that removes decay heat by air natural convection and assessed its cooling performance experimentally. In their study, the effects of convection and radiant heat transfer were compared while the wall temperature conditions were varied. Because the wall temperature of AP600 is lower than that of sodium-cooled fast reactors (SFRs), the influence of radiation on SFR cannot be compared directly with that of radiation on AP600. A natural convection experiment was performed by reducing the scale of the reactor cavity cooling system (RCCS) in the Very High-Temperature Gas-cooled Reactor (VHTR) from KAERI, as shown in Fig. 3 [8]. Its cooling system was similar to that of RVCS and considered a scale-down effect using the Ishii–Kataoka scaling method (1/4 scale). Because the operating temperature of VHTR is higher than that of SFR, Plank number was set as a primary satisfied non-dimensional group related to radiation.

Considering the previous studies on the RVCS and heat removal systems by natural convection, a more detailed understanding of the influence related with the geometry, temperature boundary conditions, scale effect, etc. on the performance of RVCS is required. Because the RVCS have a large size and height, it needs to be scaled down to investigate the effect of natural convection heat transfer on the various parameters. To scale down the experimental apparatus, we considered three well-known scaling methods: power to volume, Ishii–Kataoka, and linear method. We chose the Ishii–Kataoka scaling method [10] because it can easily focus on height, which has an important role in natural convection [11]. In this study, therefore, we designed a scaled-down experimental apparatus to investigate the heat removal performance using the Ishii–Kataoka scaling method, which was used for modeling In MARS-KS numerical simulations. However, in our scaled-down model of RVCS, the gap size was considered to be important in the progress of scaling analysis in the Ishii–Kataoka method. Because the gap size was changed following scale down, it is the most sensitive parameter in Ref. [4].

To understand the previously described complicated heat transfer from CV (one heat source), we investigated the coupled convective and radiative heat transfer phenomena in the scaled-down model. While developing the scaled-down model, we assumed that the transferred radiative heat from CV to SP changes to convective heat from SP to air in the riser channel under steady-state, as previously described. To accurately predict the heat removal rate of RVCS, the modified Richardson number was selected for a primary, focused nondimensional group for similarity ($Ri_R = 1$) related to air velocity and the air temperature difference between the inlet and outlet. Then, another nondimensional group, i.e., friction number (F/A_i^2), was included in the momentum equation with the Richardson number to set an additional

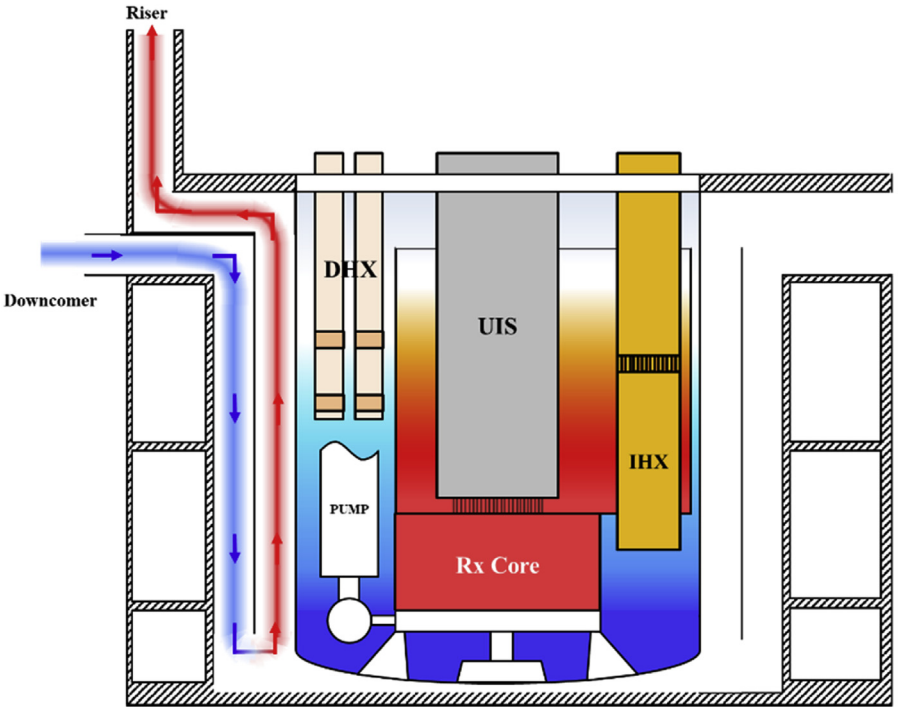

Fig. 1. Schematic image of the reactor vessel cooling system (RVCS).

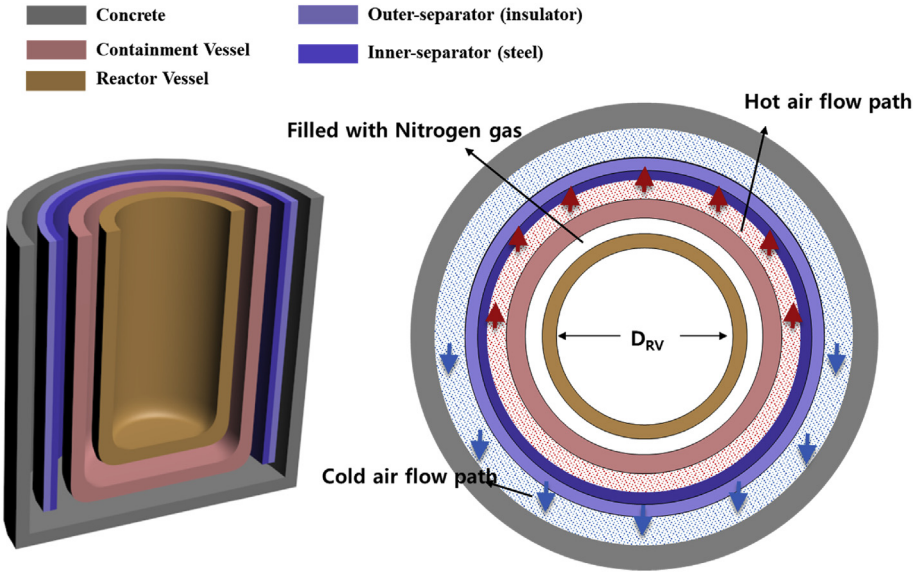

Fig. 2. Side view and top view of reactor vessel cooling system.

similarity ($\sum (F/A_i^2)_R = 1$). However, one parameter, the form loss (K), which makes up the nondimensional friction number, would remain unknown. When the modified Richardson number was used in the similarity group, the average velocity of the air in the heated riser channel of the model would be different compared with that of the prototype; i.e., the ratio of the average velocities would not be unity ($u_R \neq 1$) because of differences in height between the prototype and model ($l_R \neq 1$). Therefore, the friction factor, which depends on air velocity, would change, thus requiring the form loss coefficient to be modified to maintain similarity between the nondimensional friction numbers. Therefore, we conducted a numerical simulation using the MARS-KS code to obtain the form loss coefficient of the model. The form loss coefficient of the model was determined by conducting a parametric study in the range from 0 to 4 in the scaled-down model. When the proper heat flux, diameter (gap distance), and height of the model were set as input based on the scaling analysis, we confirmed that the prescribed air velocity and temperature ratio between the prototype and model agreed well in the case of K = 2.0, similar to the description in Section 2. Finally, we verified the result of the MARS-KS simulation based on the scaled-down model, which would be the rule of the scaled-down geometry of experimental apparatus. The results of the experiment could validate the numerical results and could prove the reliability of the scaled-down model.

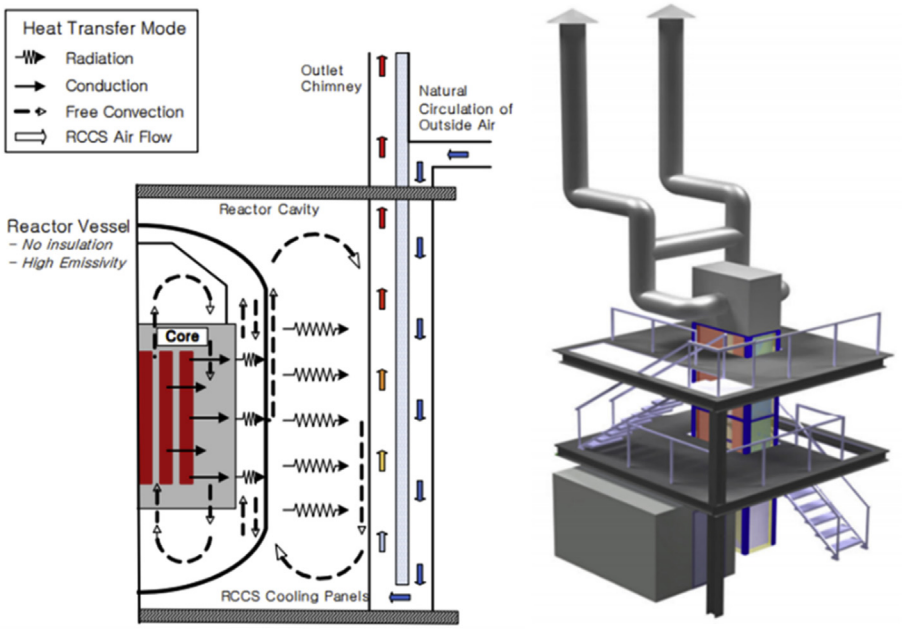

Fig. 3. Heat transfer mechanism and schematic image of RCCS [9].

2. Development of scaled-down RVCS model

2.1. Non-dimensional governing equations

To establish the scaled-down model of RVCS in this study, the governing equations of continuity, integral-momentum, and energy were nondimensionalized. The heat transfer phenomena in the downcomer were not considered because we assumed that the outer SP facing the downcomer must be adequately insulated to prevent the heat losses from the downcomer side of the outer SP to the downward airflow. The heat transferred from the reactor vessel (RV) to the CV was assumed to be a boundary condition on the CV, and we only considered the heat transfer in the vertical heated channel (riser-channel between the CV and the inner SP). Furthermore, we ignored the tropospheric bottom geometry of the CV and considered the RVCS to be a simplified U shape. Because we focused on thermal-hydraulic analysis in the vertical heated channel (riser), the proposed scaling down model could reflect the overall thermal-hydraulic phenomena and could be verified by numerical and experimental assessments.

First, the one-dimensional conservation equations (Eqs. (1) and (2) in this study took the following forms from Ishii–Kataoka [10]. Because it would be reasonable to consider that the riser is a one-dimensional object with airflow in an upward direction, the governing equations used were also one dimensional for the development of the scaled-down model. Because scaling analysis focuses on predicting the system-wide phenomena and cooling performance of the RVCS using mean values rather than local phenomena based on local values, we used the integral momentum equation and took the heated section between CV and SP as reference in this study. The main assumptions were a steady-state, negligible viscous dissipation, no volumetric heat generation, and incompressible flow using Boussinesq's approximation. We assumed that viscous dissipation could not significantly affect natural convection [12]. We set the average air velocity inside the heated channel as the reference velocity based on Eqs. (1) and (2). The subscript *i* denotes system components such as the inlet (intake pipe; downcomer with downward direction of airflow) and the outlet (discharge pipe with upward direction of airflow); the heated section is expressed as subscripted *r*.

Continuity equation

$$u_i = \frac{a_0}{a_i} u_r \tag{1}$$

Integral momentum equation

$$\rho \frac{du_r}{dt}\left(\sum_i \frac{a_0}{a_i} l_i\right) = \rho g \beta \Delta T l_h - \frac{\rho (u_r)^2}{2} \sum_i \left(\frac{fl}{d} + K\right)\left(\frac{a_0}{a_i}\right)^2 \tag{2}$$

Fig. 4 shows the heat transfer mechanism in RVCS. The air in the

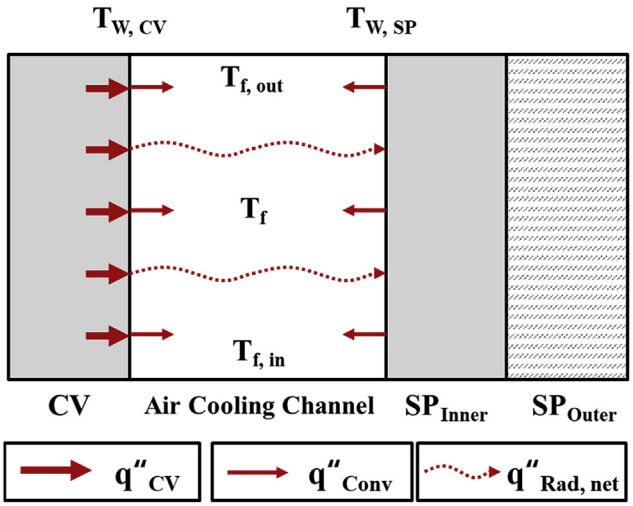

Fig. 4. Heat transfer mechanism in the riser channel of RVCS.

riser section was heated by one heat source (thick arrow). From the heat source, the air in the riser section was heated by convective heat (thin arrow), and the SP was heated by radiative heat (dot wave arrow) from the CV wall to the inner SP wall. This radiative heat turned into convective heat from the SP to air under steady-state conditions based on the assumption that the outer SP maintained the heat inside the riser channel by thermal insulation. As a result, the air was heated simultaneously by convective heat transfer mode from the both CV and SP walls. The heat transfer rate from CV (heat source) was equal to the enthalpy rise of air in the riser section from the inlet (in) to the outlet (out).

The total heat transferred from CV (Q_{CV}) was separated into convective ($Q_{Conv,\ CV}$) and the radiative ($Q_{Rad,\ CV}$) heat, as described above. Here, we developed a new energy balance model, given by Eq. (3), by converting radiative heat into convective heat from the SP to the upward air flow, assuming that the outer SP was fully insulated under steady-state conditions. The energy balance equation can be defined as follows:

$$Q_{CV} = Q_{Conv,CV} + Q_{Rad,CV} = Q_{Conv,CV} + Q_{Conv,SP} \tag{3}$$

Because the effect of radiation was not considered in the Ishii–Kataoka method [10], partially independent scaling analysis with the Ishii–Kataoka method would be required in this study. Especially, the energy equation for fluids (Eq. (4)) and the boundary conditions (Eq. (5)) used in the Ishii–Kataoka method could not be applied directly in this study to consider radiative heat transfer. Therefore, Eqs. (4) and (5) were partially modified to Eqs. (6) and (7). In the fluid energy equation (Eq. (6)), we modified the first term on the right-hand side to reflect the geometric difference (annulus) and added one similar term to consider the effect of conversion of radiative heat to convective heat by Eq. (3). In the boundary condition for CV (Eq. (7)), we added the second term on the right-hand side so that we could include the transferred radiative heat from the CV wall to the inner SP wall, which was already considered as the added term on the right-hand side in Eq. (6). Based on the energy balance (Eq. (3)), the net radiative heat flux transferred to SP could be converted to the convection heat flux on the SP under the assumption that the outer SP was fully insulated and under steady-state conditions (Eq. (8)).

Energy equation for fluid used in the Ishii–Kataoka method [10]

$$\rho C_p\left\{\frac{\partial T}{\partial t}+u\frac{\partial T}{\partial z}\right\}=\frac{(a_h)}{(v_f)}q^{''}_{conv}=\frac{\pi dl}{\left(\pi d^2/4\right)l}h\left(T_s-T_f\right)=\frac{4h}{d}\left(T_s-T_f\right) \tag{4}$$

Boundary conditions used in the Ishii–Kataoka method [10]

$$-k_s\frac{\partial T_s}{\partial y}=q^{''}_{conv}=h\left(T_s-T_f\right) \tag{5}$$

Energy equation for fluid

$$\begin{aligned}\rho C_p\left\{\frac{\partial T}{\partial t}+u\frac{\partial T}{\partial z}\right\}&=\frac{(a_{CV})}{(v_{Riser})}q^{''}_{conv,CV}+\frac{(a_{SP})}{(v_{Riser})}q^{''}_{conv,SP}\\&=\frac{(\pi d_{CV}l)}{\left(\pi d_{SP}^2-d_{CV}^2/4\right)l}h_{CV}\left(T_{CV}-T_f\right)+\frac{(\pi d_{SP}l)}{\left(\pi d_{SP}^2-d_{CV}^2/4\right)l}h_{SP}\left(T_{SP}-T_f\right)\\&=\frac{(4h_{CV}d_{CV})}{\left(d_{SP}^2-d_{CV}^2\right)}\left(T_{CV}-T_f\right)+\frac{(4h_{SP}d_{SP})}{\left(d_{SP}^2-d_{CV}^2\right)}\left(T_{SP}-T_f\right)\end{aligned} \tag{6}$$

Boundary conditions for CV

$$-k_{CV}\frac{\partial T_{CV}}{\partial y}=q^{''}_{conv,CV}+q^{''}_{rad,CV}=h_{CV}\left(T_{w,CV}-T_f\right)+q^{''}_{rad,CV} \tag{7}$$

Boundary conditions for SP

$$-k_{SP}\frac{\partial T_{SP}}{\partial y}=q^{''}_{rad,SP}=-q^{''}_{rad,CV}\frac{a_{CV}}{a_{SP}}=q^{''}_{conv,SP}=h_{SP}\left(T_{SP}-T_f\right) \tag{8}$$

Because we focused on predicting the thermal-hydraulic behavior of air in the riser section developed by natural convection, the nondimensional parameters, such as velocity of each section (U_i), velocity of the representative (heated) section (U_r), height of each section (L_i), height of the heated section (L_h), temperature difference (θ), time (τ), and area (A_i), were selected to analyze behavior of the system, as shown in Eq. (9) [10]. The subscript o represents the reference value.

Non-dimensional parameters

$$\begin{aligned}&U_i=u_i/u_o,\ \ U_r=u_r/u_o\\&L_i=l_i/l_o,\ \ L_h=l_h/l_o,\\&\theta=\Delta T/\Delta T_o\\&\tau=tu_o/l_o,\ \ A_i=a_i/a_o\end{aligned} \tag{9}$$

We then converted the governing equations of Eqs. (1), (2) and (6) into non-dimensional forms based on the nondimensional parameters in Eq. (9) as shown in Eqs. (10)–(12), respectively.

Non-dimensional continuity equation

$$U_i=U_r/A_i \tag{10}$$

Non-dimensional integral momentum equation

$$\frac{dU_r}{d\tau}\left(\sum_i\frac{L_i}{A_i}\right)=\left(\frac{g\beta\Delta T_0 l_0}{u_0^2}\right)(\theta_h-\theta_c)L_h-\frac{(U_r)^2}{2}\sum_i\left(\frac{F_i}{A_i^2}\right)^2 \tag{11}$$

Non-dimensional energy equation for liquid

$$\begin{aligned}\left\{\frac{\partial\theta_f}{\partial\tau}+\frac{U_r}{A_i}\frac{\partial\theta_f}{\partial Z}\right\}&=\left\{\frac{4h_{CV}d_{CV}}{\rho C_p u_o\left(d_{SP}^2-d_{CV}^2\right)}\right\}\left(\theta_{w,CV}-\theta_f\right)\\&+\left\{\frac{4h_{SP}d_{SP}}{\rho C_p u_o\left(d_{SP}^2-d_{CV}^2\right)}\right\}\left(\theta_{w,SP}-\theta_f\right)\end{aligned} \tag{12}$$

From the nondimensional governing equations, we extracted three nondimensional groups, which were the modified Richardson number ($Ri^*\# = g\beta(T_{Air,Out} - T_{Air,In})/u^2$), friction number ($\sum(F/A_i^2)$) in the nondimensional integral momentum equation, and the modified Stanton number in the nondimensional energy equation for fluids.

As shown in Eq. (13), The modified Richardson number denotes the ratio of the buoyancy force to the inertial force and was chosen to consider the system-wide behavior rather than the local phenomena by replacing the temperature difference between the wall and the fluid ($\Delta T = T_{Wall} - T_{Air}$) used in the well-known Richardson number ($Ri\# = g\beta(T_{Wall} - T_{Air})/u^2$) with the difference in the air temperature between the inlet and the outlet ($\Delta T = T_{Air,Out} - T_{Air,In}$). The friction number is shown in Eq. (14). It denotes the ratio between friction force and inertial force and was considered along with the modified Richardson number in the integral momentum equation to compensate for the loss of friction related with the friction factor (f) and form loss coefficient (K). Finally, we modified the Stanton number as shown in Eq. (15) using the geometry of the RVCS different from the original form in Eq. (4), although we maintained the physical meaning of the ratio between the heat transfer rate and the heat capacity.

Modified Richardson number ($Ri^*\#$)

$$Ri^* = \left(\frac{g\beta\Delta T_0 l_0}{u_0^2}\right) = \left(\frac{Buoyancy}{Inertia}\right) \tag{13}$$

Friction number

$$\sum_i \left(\frac{F_i}{A_i^2}\right) = \left(\frac{fl_o}{d_o} + K\right) = \left(\frac{Friction}{Inertia}\right) \tag{14}$$

Modified Stanton number (St#)

$$St = \left(\frac{4hd}{\left(d_{CV}{}^2 - d_{SP}{}^2\right)\rho C_p u_o}\right) = \left(\frac{Wall\ \ convection}{Axial\ \ convection}\right) \tag{15}$$

2.2. Scaling analysis

We performed a scaling analysis to identify the ratios of the variables of the model and the prototype. The ratio between the model and prototype is denoted as R as follows.

$$\Pi_R = \frac{\Pi_{\text{model}}}{\Pi_{prototype}} \tag{16}$$

The main purpose of this study was to predict the heat removal performance of the RVCS using a scaled-down model. Therefore, we concentrated on predicting the air-flow rate, which is induced by the buoyancy force based on the temperature difference of air between the inlet and outlet and by friction forces due to the geometry effect. Initially, we considered the ratio of the temperature difference between the inlet and outlet to be 1, as shown in Eq. (17). The similarities of the heat transfer media were satisfied by applying the same air properties in Eq. (18). Accordingly, we used a modified Richardson number to satisfy the similarity. The modified Richardson number is directly related to the flow rate and the temperature difference between the inlet and outlet, as shown in Eq. (13). Hence, a simple relationship between the average velocity and length between the model and prototype could be developed using Eq. (17)–(20).

$$\Delta T_R = \left(T_{f,out} - T_{f,in}\right)_R = 1 \tag{17}$$

$$\rho_R = (C_p)_R = \beta_R = 1 \tag{18}$$

$$Ri_R = \left(\frac{l_0}{u_0^2}\right)_R = 1 \tag{19}$$

$$l_{0,R} = u_{0,R}^2 \tag{20}$$

To preserve the similarity of the modified Richardson number, however, the friction number must be preserved in Eq. (21), simultaneously. Because the friction number is only a geometrical parameter, it is well-known that similarity can be ensured experimentally by using orifices or dampers [10].

$$\sum \left(\frac{F}{A_i^2}\right)_R = 1 \tag{21}$$

Because the energy balance equation between the increased enthalpy of air and the heat transfer rate is valid in the scaling analysis, the similarity of energy balance would be maintained as follows:

$$\begin{aligned} Q_R &= \left(\rho a_o u_o C_p \Delta T_f\right)_R = \left(q_w'' a_w\right)_R = 1 \\ &= \rho_R \left(\frac{\pi d_o^2}{4}\right)_R u_{o,R} C_{p,R} \Delta T_{f,R} = q_{w,R}''(\pi d_o l_o)_R \end{aligned} \tag{22}$$

Based on Eq. (17)–(20), Eq. (22) can be substituted into Eq. (23), and the heat flux ratio can be determined as follows:

$$(q_w'')_R = \frac{u_{0R} d_R}{l_{0R}} = \frac{d_R}{l_{0R}{}^{0.5}} \tag{23}$$

However, one equation is still needed to establish complete relations between the nondimensional heat flux, length, diameter, and velocity. Thus, the additional physical relation of natural convective heat transfer was applied to the scaling analysis, as shown in Eq. (24), which was an empirical heat transfer correlation with asymmetric iso-flux conditions with heating on one side and insulation on the other [13].

Under steady-state conditions, the ratio of the Stanton number should maintain its value as 1 because of the meaning of this nondimensional number. Using this result, we could obtain the relationship between the ratio of diameter and height, as shown in Eq. (26). Consequently, the relations among the ratios of parameters (u_{rn}, l_{0R}, d_{oR}, $q_{w\,R}''$) could be determined as shown in Eq. (27).

$$Nu_{o,L} = \left(\frac{q_w''}{T_{w,L} - T_\infty}\right)\frac{d}{k} = h\frac{d}{k} = 0.204\left(Ra_o^* \frac{d}{l}\right)^{0.5} \tag{24}$$

$$Ra_o^* = \left(\frac{g\beta q_w'' d^4}{k\alpha\upsilon}\right) \tag{25}$$

$$St_R = \left(\frac{hl_0}{u_0 d_0}\right)_R = \left(\frac{hl_0{}^{0.5}}{d_0}\right)_R = \left(\frac{d_{0R}}{l_{0R}^{1/4}}\right) = 1 \tag{26}$$

$$l_{0R} = (u_{0R})^2 = (d_{0R})^4 = \left(q''_{w,R}\right)^{-4} \quad (27)$$

Based on these results, we determined the height ratio by considering the applicable lab scale. The height of the prototype was estimated to be 6.7 m, except for the CV hemispheric geometry with reference to Ref. [5]. Because the diameter (gap size in this study) is the most sensitive parameter for scaling analysis as previously described in the Introduction and the height was related to the 4th power of the diameter, we decided the height to be as large as possible in the lab scale. Therefore, the available maximum height for the heated section with minimization of the effect of gap size was determined to be 3.0 m, excluding the marginal space used to support the structure, the insulator at the bottom, and the top of the experimental apparatus. As the model height was set to 3 m with the prototype height of 6.7 m, the ratio of height was determined to be 0.45; thus, the ratios of the heat flux, the flow velocity, and the diameter between the scaled-down model and prototype were determined to be 1.22 and 0.67 using Eq. (27), respectively. Finally, Table 1 shows the calculation results of each ratio such as height, diameter (gap size), air velocity, and the heat flux, and the scaled-down values of height and diameter. Selected parameter ratios of the model and prototype denote bold in Table 1.

3. Determination of form loss coefficient using MARS-KS simulation

We validated the proposed model by performing MARS-KS simulations under uniform heat flux conditions for both the prototype and the scaled-down model. MARS code is a safety analysis code related to thermal-hydraulic systems in nuclear reactors [14]. It aims to predict the thermal-hydraulic conditions of systems by solving conservation equations on the system scale based on an one-dimensional approach. Thus, the method is useful for simple geometries like that of the RVCS model.

We compared the heat removal performance of the prototype and the RVCS model. In MARS-KS, the air flow path was modeled as a riser pipe (201), where the air was heated by convection in the CV and the SP with the basic assumption shown in Eq. (3), a downcomer pipe (100) through which the air flowed under full insulation conditions, a horizontal pipe (101) connecting the downcomer to the riser, and a discharge pipe (202). In the case of the discharge pipe, the form loss coefficient could be set individually, assuming that a damper was installed to satisfy the similarity in the friction number. To suppress the flow caused by the pressure head effect, we set the height of the discharge and downcomer pipes to be the same. Although the flow path was maintained, for calculating heat structure, we considered the radiation heat transfer as one of the heats from CV to SP based on the assumption that the system is an enclosure, as shown in Fig. 5. Therefore, we included an additional heat structure at the outlet of the horizontal pipe and the inlet of the discharge pipe. Radiative heat was calculated based on the temperature of some surface to the temperatures of the remaining surfaces by assuming an enclosure.

Assuming that the metal plate constituting the wall is polished well, the emissivity of the CV and SP wall was set to 0.15 and 0.2, respectively [13]. The form loss coefficient for the shape was determined by referring to the ASHRAE Handbook [15], and the input values are summarized in Table 2.

The heat flux was estimated to be 3.4 kW/m^2 for the prototype CV heat flux, based on the RVCS design of the CV diameter (8.9 m) and height (13.5 m), and the assumed RVCS heat removal rate was approximately 1.8 MW$_{th}$ based on a previous study [16].

The heat transfer correlations of the MARS-KS are based on the natural convection heat transfer correlation in Eq. (28) in the vertical plane [17].

$$Nu = \left\{ 0.825 + \frac{0.387 Ra^{\frac{1}{6}}}{\left[1 + \left(\frac{0.492}{\mathrm{Pr}}\right)^{\frac{9}{16}}\right]^{\frac{8}{27}}} \right\} \quad (28)$$

The radiation heat flux is calculated as follows [14]:

Table 1
Different models based on the scaling law.

l $_R$	l [m]	d $_R$	d [m]	u $_R$	q"$_R$
0.10	0.67	0.56	0.17	0.32	1.78
0.30	2.01	0.74	0.22	0.55	1.35
0.45	3.00	**0.82**	0.25	**0.67**	**1.22**
0.60	4.02	0.88	0.26	0.77	1.14
0.75	5.03	0.93	0.28	0.87	1.07
0.90	6.03	0.97	0.29	0.95	1.03
1.00	6.70	**1.00**	0.30	**1.00**	**1.00**

Note – According to the ratio of height (l_R) of 0.45, the ratio of diameter (gap size), air velocity, and heat flux could be determined using Eq. (27).
The upper bold(l_R=0.45) indicates the selected scaled-down ratio and the lower bold(l_R=1.00) indicates the ratio of the prototype.

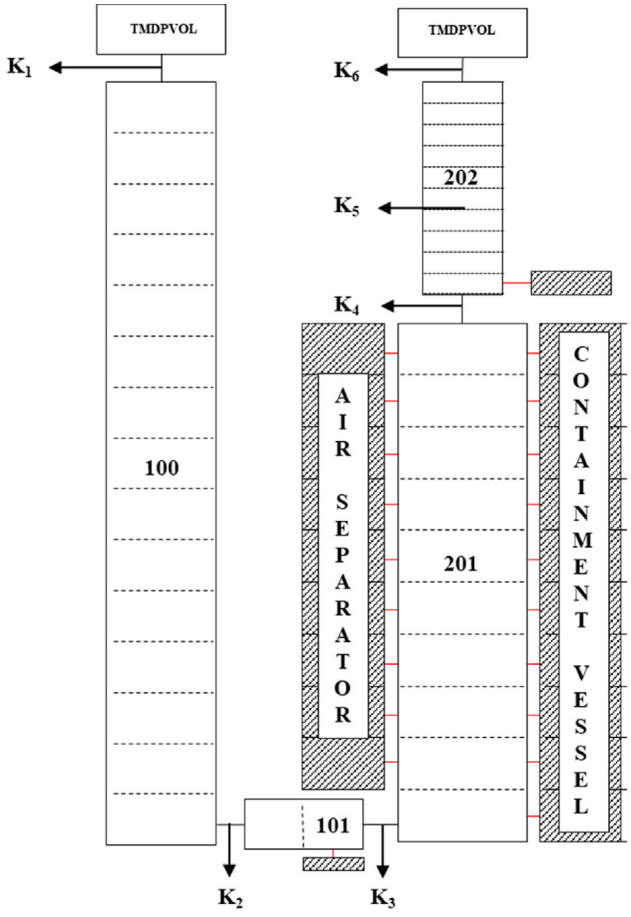

Fig. 5. RVCS model nodalization in multi-dimensional analysis of reactor safety-KINS standard (MARS-KS).

Table 2
Detailed input data for MARS-KS simulations.

Component #	Type	Prototype		Scale model		Roughness (ε)
		D [m]	L [m]	D [m]	L [m]	[m]
100	Pipe	0.25	8.20	0.25	4.50	9e-5
101		0.25	1.50	0.25	1.50	
201		0.30	6.70	0.27	3.00	
202		0.10	0.50	0.10	0.50	

Component #	Type	Form loss		Section	
		Prototype	Model	K_i	Function
200	SNGLJUN	0.80	0.80	K_1	Entrance
300		0.20	0.20	K_2	90° Bend
400		1.75	1.75	K_3	Expansion
500		0.93	0.93	K_4	Contraction
202 (4th)	Pipe JUN	0.00	0–4.0	K_5	Damper
600	SNGLJUN	1.00	1.00	K_6	Exit

Component #	Type	Prototype		Model		Material
		Heat flux [kW/m^2]	Length [m]	Heat flux [kW/m^2]	Length [m]	
1001	Heat structure	3.406	6.70	4.155	3.00	SUS
1002		–	6.03	–	2.70	
1003		–	0.30	–	0.245	
1004		–	0.73	–	0.387	

$$q_i^{''} = R_i - \sum_{j=1}^{n} R_j F_{ij} = \frac{\varepsilon_i}{\rho_i}\left(\sigma T_i^4 - R_i\right) \tag{29}$$

To assess the validity of the scaled-down model obtained from our scaling analysis, we compared the ratio of the average velocity ($u_{o,R} = 0.67$) and temperature difference of the outlet and inlet ($\Delta T_{o,R} = 1$) between the prototype and scaled-down model by varying the form loss coefficients ($0 \le K \le 4$) at increments of 0.5 for the scaled-down cases.

Fig. 6 shows that the difference in air temperature between the prototype and scaled-down model is the most similar in the case when K = 2.5. The temperature difference ratio, which is related to the buoyancy effect, was equal to 1.004, which is very similar to the induced temperature difference ratio ($\Delta T_{o,R} = 1$). In terms of the average velocity ratio, we confirmed that the flow velocity ratio was 0.669 in the case of K = 2.0, which is the most similar to the induced average velocity ratio ($u_{o,R} = 0.67$).

According to the results of our comparison between the modified Richardson number of the prototype and the scaled-down models for various form loss coefficients, the deviation was less than ±15% for form loss coefficients between 1.5 and 2.5 (Fig. 7).

After comparing the ratio of the temperature difference between the inlet and outlet ($\Delta T_{o,R} = 1$), the average air velocity ratio in the heated section ($u_{o,R} = 0.67$), and the prescribed modified Richardson number ratio ($Ri_R^* = 1$), based on the results of MARS-KS simulation, we found that the case of K = 2.0 had the least root mean square error of 3.0% considering overall errors; a ratio of velocity of 0.0%; a temperature difference of 4.2%, and a modified Richardson number of 3.3% between the prototype and model. Thus, K = 2.0 was found to be the most suitable value in this study, as shown in Table 3.

When the flow rate and temperature of the system vary in the process of scaling down, we need to check that the flow regime (laminar/turbulent) does not change according to the numerical analyses on the scaled-down model and the prototype. To check the flow regime under natural convection, we compared the Rayleigh numbers (Ra_L) of the prototype and the scaled-down model. We confirmed that both of the prototype and scaled-down models exceeded the critical Rayleigh number (~10^9), which is commonly known to be the criterion of turbulent flow in natural convection

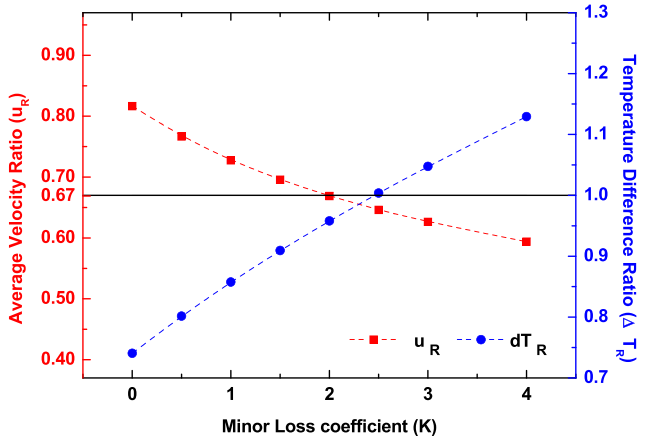

Fig. 6. Comparison between the average velocity ratio and the temperature difference ratio.

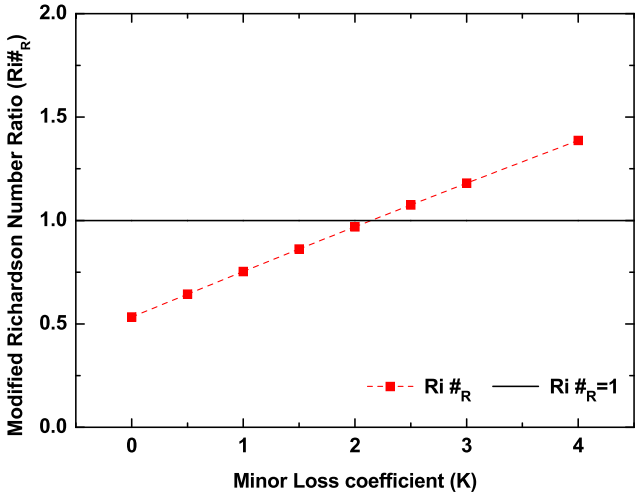

Fig. 7. Comparison between the modified Richardson number ratio.

along vertical plates. Therefore, we could confirm the validity of the proposed scaled-down model in the turbulent regime on natural convection. In addition, Reynolds number (Re_D) of the scaled-down model and the prototype were exceeded the critical Reynolds number ($Re_{d,\ critical}$~ 2300), which is the criterion to judge the laminar-turbulent transition.

However, Fig. 8 shows that the summation of the friction numbers on each section had a difference of up to 22% as the form loss coefficient increased in the case of K = 2.0. Because the area term ($A_i^2 = (a_i/a_o)^2$) in terms of friction number includes the square of the ratio of areas and increases exponentially, the area term would dominate the friction number rather than the F ($= fl/d + K$) between the scale model and the prototype. Therefore, the section in which the area changes from the prototype to the model in the process of the scaling analysis should be considered carefully to ensure fully satisfied similarity along with the modified Richardson number, even if each section is not related to the heated section.

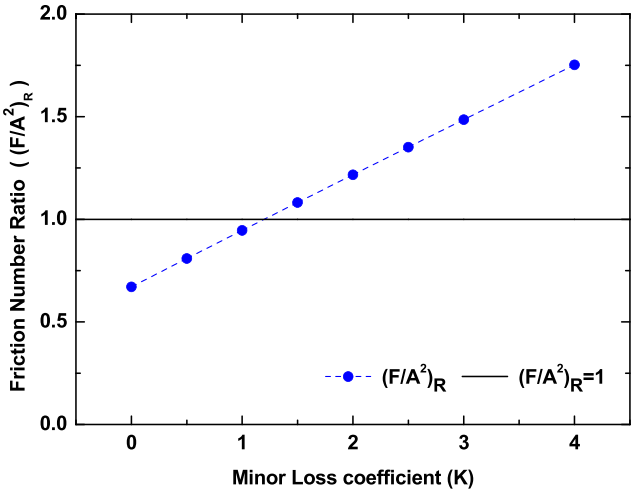

Fig. 8. Comparison of the friction number ratio.

4. Comparison of results of the MARS-KS code simulation between the prototype and scaled-down model

We compared the temperature distribution of the CV, SP, and the air in the riser and average velocity distribution with respect to the height of the prototype and that of the scaled-down model ($K = 2.0$). As shown in Figs. 9 and 10, the height of the prototype and scaled-down model were nondimensionalized, respectively, to compare the results. The air temperature and flow velocity could be reasonably predicted; however, the wall temperatures of the CV and SP slightly differed between the prototype and the model. The heat flux condition of the scaled-down model is 1.22 times higher than that of the prototype, which is determined based on the scaling analyses ($q_R^{''} = 1.22$). In addition, the air velocity ratio predicted by the MARS-KS code between the scaled-down model and the prototype was similar with the estimated velocity ratio ($u_R = 0.67$). Thus, the wall temperature of the scaled-down model became higher.

We compared the ratio of the radiative heat flux to the convective heat flux on the CV wall, which was 0.73:0.27 in the case of the prototype and thus was similar to that of the scaled-down model, 0.71:0.29, as shown in Fig. 11. This means that the scaled-down model was reliable in terms of similitude to the prototype with the ratio of heat amount between radiation and convection. Since the wall temperatures of the CV and SP increased simultaneously, it would be supposed that the fractions between the radiation and convection of the scaled model could be very close to that of the prototype even with the highest wall temperature of 553.93 °C.

A comprehensive assessment of the results described above could confirm that the scaled-down model with K = 2.0 could be selected as the representative scaled-down model to predict the

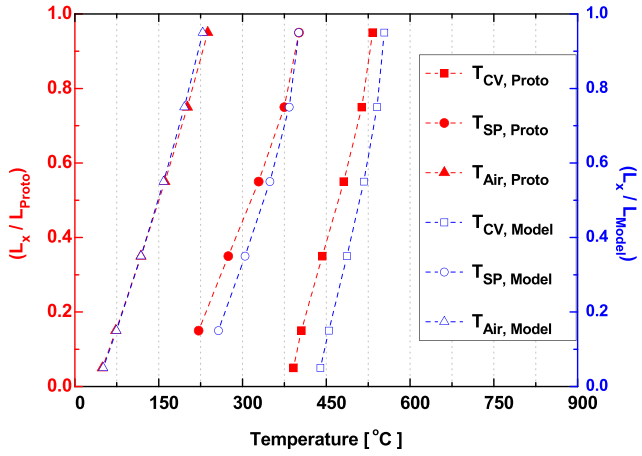

Fig. 9. Comparison of the result of axial temperature distributions between the prototype and model by MARS-KS.

natural convective heat transfer and the radiative heat transfer in RVCS. Although the wall temperature and the air velocity along the height (l) were slightly different between the prototype and the scaled-down model, these results indicate that the proposed scaled-down model could adequately predict the thermal-hydraulic phenomena systemically with complex conditions such as coupled radiative and convective heat transfer. In terms of evaluation of the reliability of nuclear power plants (NPPs) in this study, the result with slightly higher wall temperature could be more conservative because the system temperature such as that of the RV would be predicted to be higher.

Table 3
Simulation results of the different cases.

	l_R	d_R	q''_R	u_R (Error)	$\triangle T_R$ (Error)	$Ri\ \#_R$ (Error)	E_{RMS}	Ra_L	Re_D
Prototype	1 (6.7 m)	1 (0.3 m)	1 (3.4 kW/m^2)	1	1	1	–	–	–
Model	0.45 (3.0 m)	0.82 (0.25 m)	1.22 (4.2 kW/m^2)	0.669	1	1	–	–	–
MARS (Prototype)	1 (6.7 m)	1 (0.3 m)	1 (3.4 kW/m^2)	–	–	–	–	3.46e12	4554
MARS (K = 1.5)	0.45 (3.0 m)	0.82 (0.25 m)	1.22 (4.2 kW/m^2)	0.696 (4.0%)	0.909 (9.1%)	0.860 (14.0%)	9.8%	1.23e11	2969
MARS (K = 2.0)				0.669 (0.0%)	0.958 (4.2%)	0.967 (3.3%)	3.0%	1.20e11	2792
MARS (K = 2.5)				0.646 (3.4%)	1.004 (0.4%)	1.073 (7.3%)	4.8%	1.18e11	2641

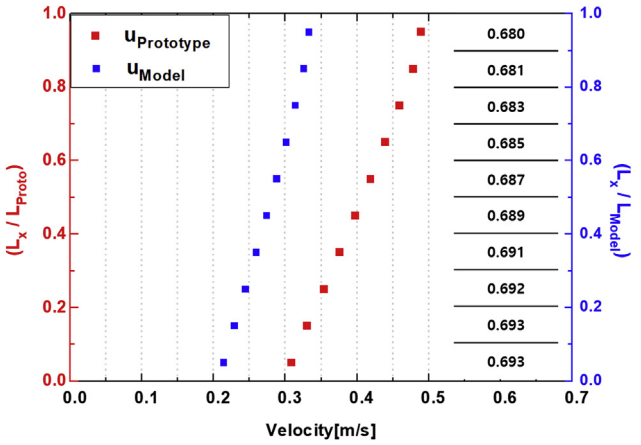

Fig. 10. Comparison of the results of average velocity between prototype and model in MARS-KS.

5. Experimental results

The experimental apparatus consisted of a downcomer, horizontal connector between the downcomer, the riser, and a heated section, as shown in Fig. 12.

The downcomer fed ambient air into the heated section. The height and diameter of the downcomer were 4.5 m and 0.25 m, respectively. To minimize the pressure loss of the inlet pipe (downcomer) and to consider only the buoyancy force of the heated section with a butterfly damper in the riser channel, the cross section of the riser (1962.5 cm^2) was chosen to be bigger than that of the heated section (735 cm^2). The connector connected the downcomer and the heated section. Its diameter was the same as that of the downcomer, and the connector was connected with a 90° degree elbow to the downcomer. A transition part (round to square (300 × 300 mm^2)) between the heated section and the connector from the downcomer was connected. The hot air flow in the heated section entered the riser by buoyancy and was discharged into the ambient surroundings in the outlet at the end of the riser. In the riser pipe, a butterfly damper was installed to consider the form loss of the system by varying the closing angle of the butterfly damper. When the damper was closed at a smaller angle, the flow friction would increase, thus decreasing the air flow rate induced by natural convection. The heated section was a flow channel of air between the vertical parallel plates, and the air inside the heated section was heated by convection on walls of both sides by simulating the CV and SP, as previously described. The height of the heated section and the gap size were 3.0 m and 0.245 m, which were determined by the scaled-down model proposed in previous sections. The 3-m high heated section was assembled using 10 metal (stainless steel, 294 × 300 mm^2) plates 10 mm in thickness. To achieve structural stability at high temperatures, tongue and groove joints were used to assemble all plates to minimize the deformation by thermal expansion (Fig. 13). The SP was composed of nine metal plates (294 × 300 mm^2), and its height was 2.7 m forming a U-shaped flow path. To change the gap size between the two vertical walls of CV and SP, the top part of the SP structure was designed to be easily modified by adopting a moving system (igus DryLin R XUMO-01-16, WS-16), as shown in Fig. 14.

Ceramic bending heaters were installed on the 10 metal plates that composed the CV. This heater can be easily attached to the plate and allows high temperature operation conditions (~800 °C) with a thermal capacity of 2.1 kW. One individual PID system controls the application of heat on two vertical plates in the heated section, and total of five PID systems were installed for independent control of both the uniform flux and uniform wall temperature of CV as the boundary conditions, as shown in Fig. 15. The uniform heat flux conditions were achieved by applying the same electric potential to each set of plates, and the uniform wall temperature

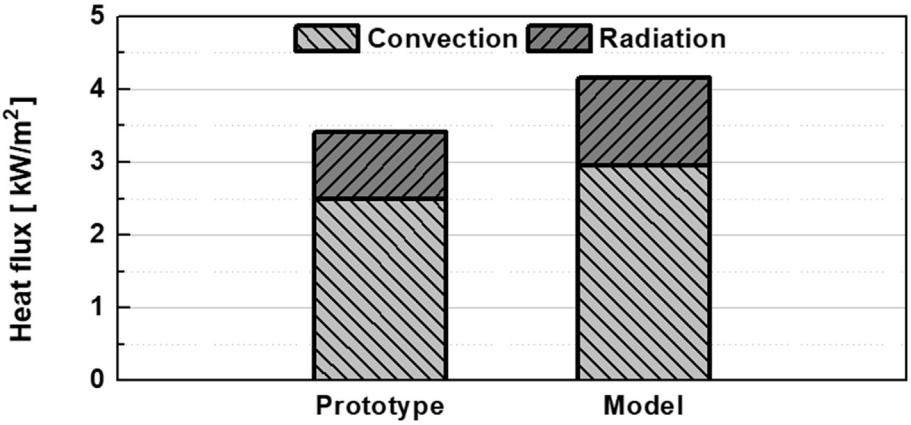

Type	q" Total	q" Conv (q" Conv/q" Total)	q" Rad (q" Rad/q" Total)
Prototype	3.406 kW/m²	2.501 kW/m² (73.4%)	0.905 kW/m² (26.6%)
Model	4.155 kW/m²	2.958 kW/m² (71.2%)	1.197 kW/m² (28.8%)

Fig. 11. Average heat flux on the containment vessel (CV) wall at different scales.

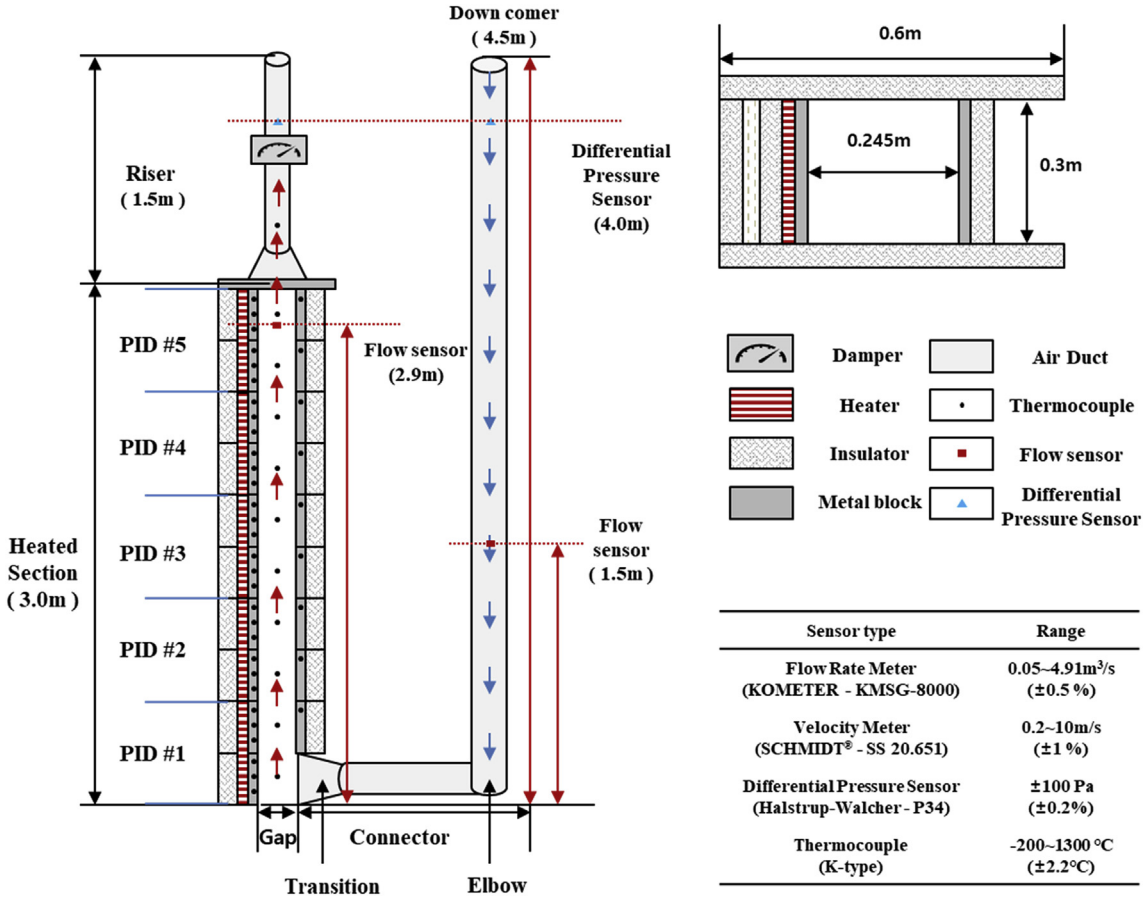

Sensor type	Range
Flow Rate Meter (KOMETER - KMSG-8000)	0.05~4.91m³/s (±0.5 %)
Velocity Meter (SCHMIDT® - SS 20.651)	0.2~10m/s (±1 %)
Differential Pressure Sensor (Halstrup-Walcher - P34)	±100 Pa (±0.2%)
Thermocouple (K-type)	-200~1300 °C (±2.2°C)

Fig. 12. Schematic of the experimental apparatus.

conditions were achieved by PID control with the wall temperature input to the heated plates. The changes in electrical properties with respect to temperature increase were neglected.

Thirty K-type thermocouples 0.5 mm in diameter were installed at 30 elevations from 0.05 m to 2.95 m with increments of 0.1 m. Three K-type thermocouples 0.5 mm in diameter were installed on each level to ensure the wall temperature of the heated plate. As shown in Fig. 12, two thermal mass flow sensors for the bulk flow rate and the local flow velocity were installed at the inlet at a height of 1.5 m in the downcomer for fully developed flow regime and at the outlet at a height of 2.9 m in the heated section. The thermal mass flow sensor measures the electric resistance at the local position and provides both the local flow velocity directly and the bulk flow rate via calculations using previously calibrated geometry information by the manufacturer. A differential pressure gauge was installed at the same height (4.0 m) between the riser and the downcomer to measure the pressure drop of air flow.

A steady-state was maintained for at least over 4 h after turning on the heating system. Because the sinusoidal fluctuation of temperature is shown in the PID control, a quasi-steady state is considered to be a steady-state when wall temperature deviation is less than 1 K and using the latest value of the SP wall temperature in several experimental cases, which should be considered for the ambient temperature changing. The heat flux on the CV wall was obtained using the energy balance between the heat removal rate and enthalpy rise, as shown in Eq. (30).

$$q''_{CV} = Q/A_{Heated} = \dot{m}C_P\Delta T/A_{Heated} = \rho A_{Cross} u C_P \Delta T/A_{Heated} \tag{30}$$

The experimental uncertainty of the heat flux was estimated using Eq. (31) [18].

$$U_{q''_{CV}} = \sqrt{\left(\frac{\partial q''_{CV}}{\partial \rho}U_\rho\right)^2 + \left(\frac{\partial q''_{CV}}{\partial A_{Cross}}U_{A_{Cross}}\right)^2 + \left(\frac{\partial q''_{CV}}{\partial u}U_u\right)^2 + \left(\frac{\partial q''_{CV}}{\partial C_p}U_{C_p}\right)^2 + \left(\frac{\partial q''_{CV}}{\partial \Delta T}U_{\Delta T}\right)^2 + \left(\frac{\partial q''_{CV}}{\partial A_{Heated}}U_{A_{Heated}}\right)^2} \tag{31}$$

The uncertainties related to material properties were estimated based on the uncertainty of the measured temperature (2.2 °C). The maximum uncertainty of the heat flux was estimated to be less than 3.5%. In addition, to ensure the highest accuracy of the temperature, all thermocouples were calibrated before the experiment using a temperature calibrator (SIKA-TP17). The measured temperature deviation among all thermocouples was less than 1.0 °C.

Although the experimental apparatus was well insulated, it would be difficult to exactly estimate the actual thermal power to

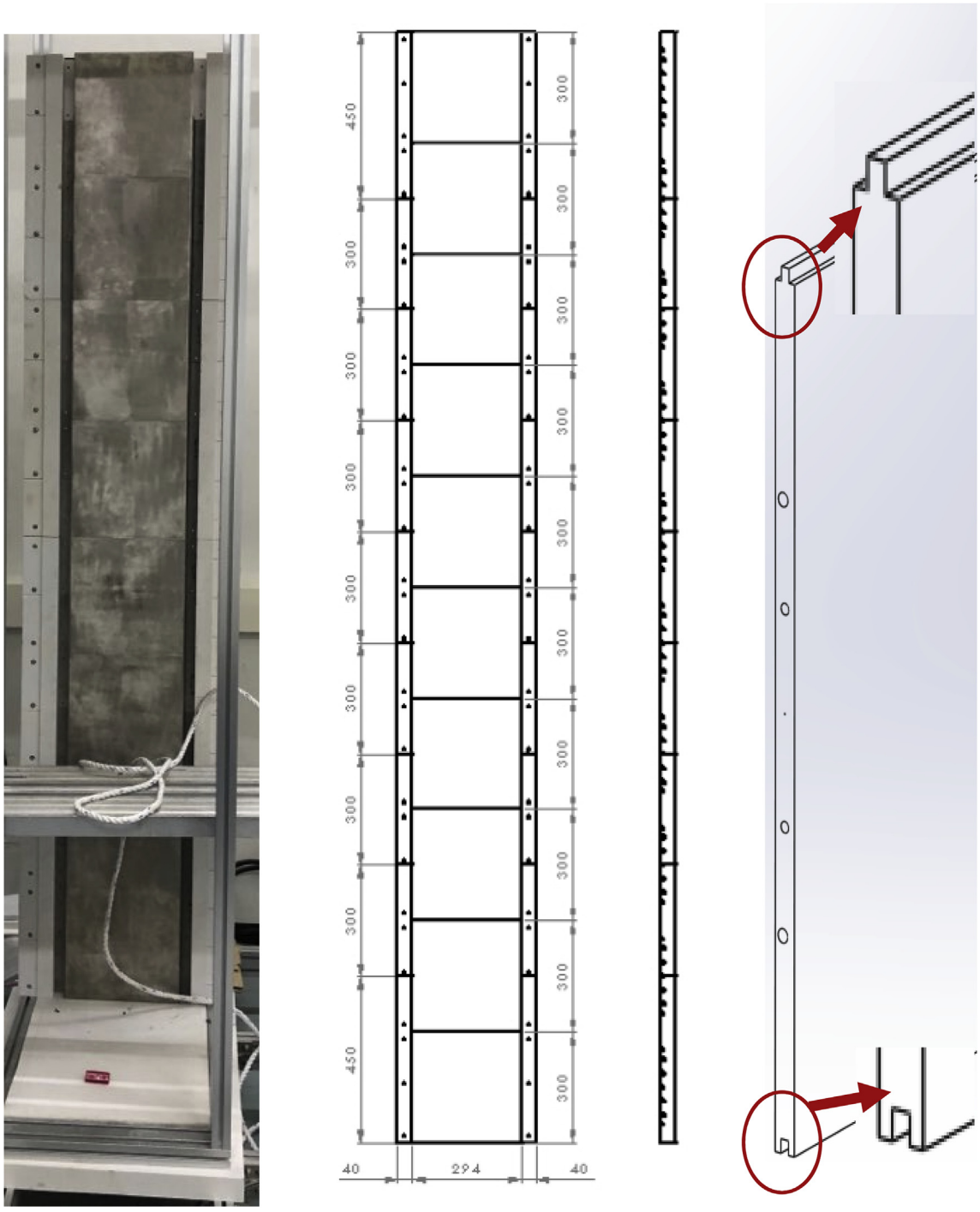

Fig. 13. Details of the directly heated wall (simulation CV).

be applied to air flow because the heat loss would vary according to the air flow rate by natural convection, which would be decided by the closing angle of the damper. Therefore, we evaluated the heat flux from CV based on the energy balance equation of air flow rate by measuring the average air temperature and the flow rate, as follows:

$$Q = \dot{m} C_p \Delta T_{air} = \dot{q}''_{CV} A \tag{32}$$

As shown in Eq. (29), we applied a radiation network approach to calculate the radiation heat flux based on the measured temperature of the CV and SP. Consequently, the convection heat rate was estimated using the total heat rate from the CV wall and the radiation heat rate as follows.

$$Q_{CV} = Q_{Conv,CV} + Q_{Rad,CV} \tag{33}$$

The experiments were performed with a 22.5° inclined angle of the damper under a uniform heat flux (4.155 kW/m^2) based on electric input power each 5 power control sections at averaged

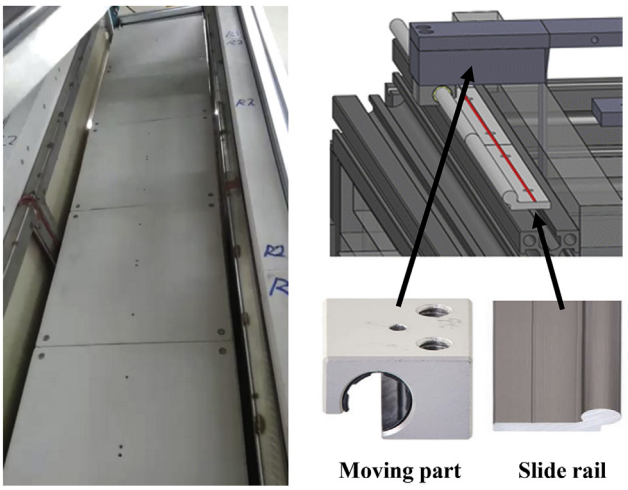

Fig. 14. Details of the indirectly heated wall (simulation SP).

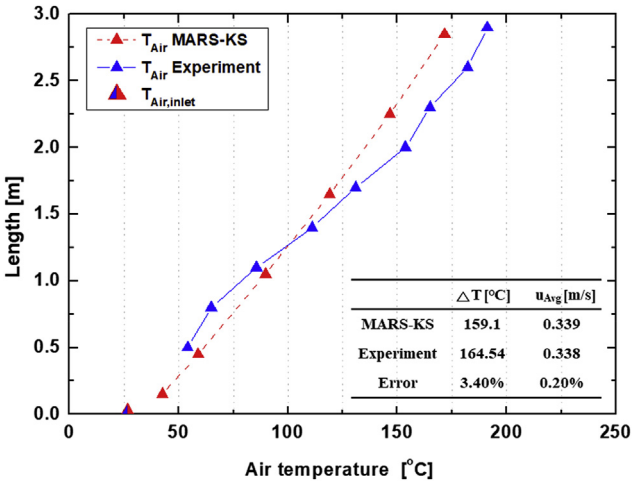

Fig. 16. Air temperature distribution of experiment and numerical simulation.

ambient air temperature of 26.7 °C, matched same condition with the MARS simulation on the scaled-down model with the case of K = 2.0. The form loss coefficient corresponding to the 22.5° inclined angle was estimated to be about 1.7, which is similar to the form loss coefficient about 2.0. We compared the results of the MARS-KS simulation with the experimental results. As shown in Fig. 16, the MARS code predicted a linear air temperature distribution, yet the experimental results showed that the temperature distribution had some inflection points. Despite this difference, the error was very small. The errors between the result of the MARS-KS and that of the experiment were 3.4% of the temperature difference between the inlet and outlet and 0.2% of the average velocity. As previously described in Sections 3 and 4, the proposed scaled-down model of geometry was determined with respect to the similitude of the thermal-hydraulic phenomenon with nondimensional numbers, the modified Richardson number, the friction number, and the modified Stanton number. In addition, the MARS-KS simulations in the previously selected geometry were conducted with various form loss coefficients ($0 \leq K \leq 4$) to estimate the unknown friction number. Finally, the form loss coefficient of the proposed scaled-down model was determined to be K = 2.0, and we designed the experimental apparatus with the given geometry information and verified the similitude of thermal-hydraulic phenomena though experiments of natural convection. As shown in Fig. 16, the experimental result shows the reliability to verify the scaled-down model which could be matched with numerical simulations of MARS-KS.

To better verify the scaled-down model, the ratio of radiative and convective heat transfer of the numerical simulation and experimental results were verified, as shown in Fig. 17. In the experimental results, the radiative heat was calculated using Eq. (29), and the experimental results of the ratio of radiative and convective heat transfer were very similar to the numerical simulation results, as previously shown in Section 4. This shows that the proposed scaled-down model can be acceptable to predict the thermal-hydraulic phenomena in RVCS. In Fig. 17, a slight difference was observed in the ratio between the numerical and the experimental results; however, this could be explained as follows. The MARS-KS code is a representative system code, which is suitable for predicting system behavior rather than local phenomena. A slight difference in the temperature distribution between the numerical and experimental results can be explained by the disagreement in the local heat transfer. In the natural convective heat transfer in the vertical parallel channel of MARS-KS, the average air velocity in each node (in experiments, it could be considered as each heated plate) was used as a parameter to calculate the heat transfer. However, the local velocity near the wall needs to be considered to calculate the heat transfer coefficient for more precise predictions. In addition, the local velocities near CV and SP would be significantly different, so that the heat transfer coefficient on the CV and SP would be different. Thus, the system code of MARS-KS could have led to the slight error with respect to the experimental results.

6. Conclusion

In this study, we proposed a numerically assisted scaling method for a vertical parallel heated channel to analyze coupled

Fig. 15. Ceramic bend heater and PID system.

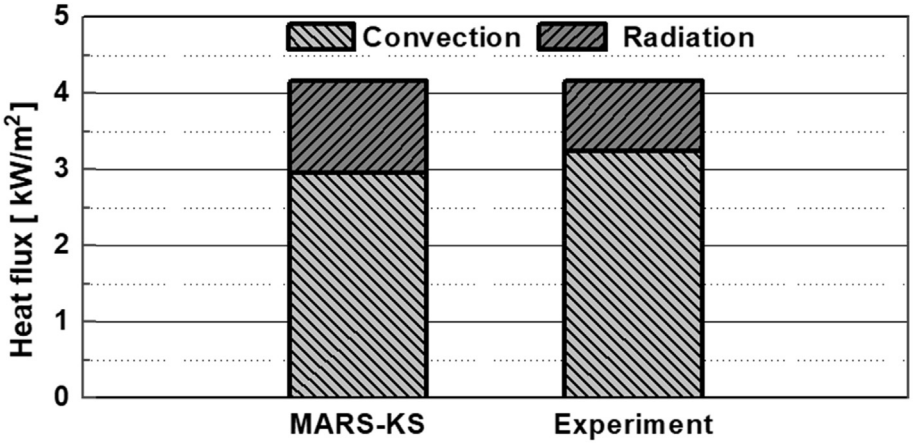

Type	q" Total (q" Conv +q" Rad)	q" Conv (q" Conv /q" Total)	q" Rad (q" Rad /q" Total)
Experiment	4.155 kW/m²	3.234 kW/m² (77.8%)	0.921 kW/m² (22.2%)
MARS-KS		2.958 kW/m² (71.2%)	1.197 kW/m² (28.8%)

Fig. 17. Comparison of results of the average heat flux in the containment vessel (CV) wall between the result of the MARS-KS code simulation and experimental result.

natural convection and radiation heat transfer modes. The scaled-down model was determined using the modified Ishii–Kataoka method. MARS-KS code simulation was conducted between the prototype and the model to estimate the form loss coefficient of the scaled-down model. Based on this result, the scaled-down model was analyzed, and the reliability of the model was verified. The detailed results of each section are summarized as follows:

- In Section 2, three nondimensional groups (modified Richardson number, friction number, and Stanton number) are derived using nondimensional governing equations (Eq.(10)–(12)). During the scaling analysis, the modified Richardson number was chosen as the nondimensional number to primarily satisfy the similarity ($Ri_R^* = 1$) for predicting the heat removal performance of RVCS. Therefore, the relation of between the parameter ratios between prototype and the model was determined (Eq. (27)). By considering the applicable lab scale, we fixed the height ratio at 0.45, and then, the ratios of the heat flux, the flow velocity, and the diameter were determined automatically to be 1.22 and 0.67, respectively.
- In Section 3, we determined the form loss coefficient of the scaled-down model by conducting MARS-KS code simulations on the prototype and the scaled-down model ($0 \leq K \leq 4$). The determined parameter ratios were compared for each case of the scale down by varying the form loss coefficient ($0 \leq K \leq 4$) with the prototype. Based on the simulation results, the scaled-down model was selected for the case of K = 2.0 because the overall error of the determined parameters was the least in this case among all cases. In addition, the flow regime between the prototype and model was checked by comparing the critical Rayleigh number and Reynolds number. However, the friction number had a difference of up to 22%. This error was dominated by the area ratio term rather than the friction term. Therefore, the cross-section area was determined carefully even if the area had no effect on heat transfer.
- In Section 4, MARS-KS code simulation results were compared between the prototype and the scaled-down model for the case of K = 2.0. The velocity in the heated section and temperature difference between the inlet and outlet were well predicted with the determined scaled-down model. However, the wall temperature of CV and SP were slightly different between the prototype and the model because the heat flux and velocity of the model were higher and lower than that of the model, respectively. Although the wall temperature of CV and SP differed between the prototype and the scaled-down model, the proposed model could predict the system well with respect to the coupled radiation and convection heat transfer modes based on the comparison results of the convective and radiative heat between the prototype and model.
- In Section 5, we experimentally verified whether the MARS-KS code results accurately agreed with the experimental results and confirmed whether it provides good estimates of the experimental results. To realize the simulated form loss coefficient of 2.0 in the experiment, the butterfly damper was set at a 22.5° inclined angle. We evaluated the air temperature distribution according to the change in height. The results of comparison showed that the temperature distribution between the experiment and numerical simulation differed slightly. Because of the velocity used for numerical calculating the heat transfer coefficient as a parameter, the average velocity was considered. However, the local velocities near CV and SP were significantly different than each other in the real phenomena.

Declaration of competing interest

The authors declare that they have no conflict of interests for financial.

Acknowledgements

This research was supported by the National Research Foundation of Korea (NRF) grant funded by the Korean government (Ministry of Science and ICT) (NRF- 2017M2A8A4018582).

References

[1] J. Yoo, J. Chang, J.-Y. Lim, J.-S. Cheon, T.-H. Lee, S.K. Kim, K.L. Lee, H.-K. Joo, Overall system description and safety characteristics of prototype Gen IV sodium cooled fast reactor in Korea, Nuclear Engineering and Technology 48 (2016) 1059–1070.
[2] C. Choi, T. Jeong, S. An, Thermal-hydraulic analyses of passive reactor vault cooling system (RVCS) in PGSFR using MARS-LMR, Ann. Nucl. Energy 117 (2018) 333–342.
[3] S. Yeom, S.H. Ryu, D. Kim, T.-H. Lee, The effect of duct level on the performance of reactor vault cooling system in the PGSFR, in: Proceedings of the KNS 2015 Fall Meeting, 2015.
[4] C. Choi, T. Jeong, S. Yeom, T.-H. Lee, K.L. Lee, Effect of ractor vault cooling system (RVCS) on reactivity feedback using MARS-LMR, in: Asian Conference on Thermal Sciences, 2017.
[5] J. Heineman, M. Kraimer, P. Lottes, D. Pedersen, R. Stewart, J. Tessier, in: Experimental and Analytical Studies of a Passive Shutdown Heat Removal System for Advanced LMRs, Argonne National Lab., 1988.
[6] X. Cheng, F. Erbacher, H. Neitzel, Passive containment cooling by natural air convection and thermal radiation after severe accidents, Nucl. Eng. Des. 202 (2000) 219–229.
[7] X. Cheng, U. Müller, Turbulent natural convection coupled with thermal radiation in large vertical channels with asymmetric heating, Int. J. Heat Mass Transf. 41 (1998) 1681–1692.
[8] Y.-Y. Bae, S.-D. Hong, Y.-W. Kim, Scaling analysis of PMR200 reactor cavity cooling system, Nucl. Eng. Des. 271 (2014) 523–529.
[9] J.-H. Kim, Y.-Y. Bae, C.-S. Kim, S.-D. Hong, M.-H. Kim, The test results of the NACEF RCCS test facility, in: Trans. Of the KNS Spring Meeting, 2015.
[10] M. Ishii, I. Kataoka, Scaling laws for thermal-hydraulic system under single phase and two-phase natural circulation, Nucl. Eng. Des. 81 (1984) 411–425.
[11] U.N.R. Commission, Compendium of ECCS Research for Realistic LOCA Analysis, NUREG-1230, Washington, DC, 1988.
[12] A. Kay, Pressure work and viscous dissipation in the equations of thermal convection in a vertical channel, J. Eng. Math. 104 (2017) 107–130.
[13] T.L. Bergman, F.P. Incropera, D.P. DeWitt, A.S. Lavine, Fundamentals of Heat and Mass Transfer, John Wiley & Sons, 2011.
[14] B.D. Chung, K.D. Kim, S.W. Bae, J.J. Jeong, S.W. Lee, M.K. Hwang, C. Yoon, MARS Code Manual Volume I: Code Structure, System Models, and Solution Methods, Korea Atomic Energy Research Institute, 2010.
[15] D.G. Colliver, T.F. Burks, R.S. Gates, H. Zhang, in: Development of the Design Climatic Data for the 1997 ASHRAE Handbook–Fundamentals, Univ. of Kentucky, Lexington, KY (US), 2000.
[16] T. Lee, T. Kim, S. Choi, S. Kim, E. Kim, J. Kim, J. Han, J. Eoh, D. Kim, J. Yoon, in: Fluid System Design of Prototype Gen-IV Sodium Cooled Fast Reactor, Korea Atomic Energy Research Institute, 2016.
[17] S.W. Churchill, H.H. Chu, Correlating equations for laminar and turbulent free convection from a vertical plate, Int. J. Heat Mass Transf. 18 (1975) 1323–1329.
[18] J.P. Holman, W.J. Gajda, Experimental Methods for Engineers, McGraw-Hill, New York, 2001.